TMS paper selection

PAPER NO.
F84-14

AN X-RAY DIFFRACTION STUDY OF TITANIUM OXIDATION

by

K. E. WIEDEMANN

J. UNNAM

THE METALLURGICAL SOCIETY OF AIME
420 Commonwealth Drive, Warrendale, PA 15086 • 412/776-9000

AN X-RAY DIFFRACTION STUDY OF TITANIUM OXIDATION

K. E. Wiedemann and J. Unnam

Analytical Services and Materials, Inc.
103 Winder Road
Tabb, Virginia 23602
USA

Abstract

Titanium specimens of commercial purity were exposed at 1100° to 1400°F to laboratory air for times up to 100 hours. The extent of substrate contamination by interstitial oxygen was determined by a new x-ray diffraction analysis involving transformation of x-ray diffraction intensity bands. The oxygen solid-solubility at the oxide-metal interface and its variation with time at temperature were also determined. Diffusion coefficients are deduced from the oxygen depth profiles.

Introduction

Oxygen forms a solid solution with α-titanium in the 0 to 34 atomic percent range (1). The α-titanium has a hexagonal-close-packed structure and the oxygen is incorporated interstitially in the octahedral lattice sites. Presence of oxygen causes the unit cell to expand, principally along the c-axis.

Holmberg (2) has determined two order-disorder reactions in the 25 to 34 atomic percent range. Anderson et al. (3) observed a reversal in the effect of oxygen on the a lattice parameter at 25 atomic percent. For compositions below 25 atomic percent the a lattice parameter lengthens with increasing oxygen content, and for compositions greater than 25 atomic percent it contracts with increasing oxygen content. Kofstad et al. (4) noted that the apparent solubility at the metal-oxide interface during oxidation does not exceed 25 atomic percent. David et al. (5), Unnam et al. (6), and Wiedemann (7) reported values near 20 atomic percent. In this paper x-ray diffraction was used, because of its accuracy and high resolution (8), to study the dissolution process.

Theory

X-ray diffraction peaks that have compositional broadening can be analyzed to determine the composition-depth profile. It can be shown that the diffraction peak is the attenuated derivative of the composition-depth profile. To obtain the profile from the x-ray intensity it is necessary to divide by the attenuation and integrate (in the proper direction) over the diffraction peak.

The power diffracted by a volume element (in a flat sample) with a thickness dx and at a depth x is given by the well known equation:

$$dP = 2P_o \delta\lambda^{-1} \exp(\eta_x) Q \, dx \tag{1}$$

where P_o is the incident power, δ is the Bragg d-spacing, λ is the x-ray wavelength, η_x is the absorption term, and Q is the pseudo-reflectivity. The absorption term is given by:

$$\eta_x = -4\delta\lambda^{-1} \int_0^x \mu \, dx \tag{2}$$

where μ is the compositionally dependent linear absorption coefficient. The pseudo-reflectivity is given by:

$$Q = \frac{r_e^2 \lambda^3}{V^2} \frac{1 + \cos^2 2\theta}{2 \sin 2\theta} F^2 \, p \exp(-2M) \tag{3}$$

where r_e is the classical radius of the electron, V is the volume of the unit cell, F is the structure factor, p is the multiplicity, and $\exp(-2M)$ is the Debye-Waller factor.

Equation (1) is used to define a modified diffracted power corrected for composition and path length as:

$$P_x = 2 \int_{\delta_o}^{\delta_x} \left(\frac{dP}{d\delta}\right) \frac{2\mu}{Q} \left(1 + \gamma_x\right) d\delta \tag{4}$$

where δ_o corresponds to the d-spacing of surface material ($x = 0$), $\left(\frac{dP}{d\delta}\right)$ is proportional to the diffracted intensity, and γ_x is given by:

$$\gamma_x = (\mu\delta)^{-1} \frac{d\delta}{dx} \int_0^x \mu \, dx \tag{5}$$

which tends to zero for all practical purposes.

It can also be seen from Eq. (1) that:

$$P_x = P_o\left[\exp(\eta_o) - \exp(\eta_x)\right] \tag{6}$$

From Eqs. (4) and (6) the depth of a diffracting volume element is given by:

$$x = \frac{-\lambda}{4} \int_{\delta_o}^{\delta_x} \mu^{-1} \frac{d}{d\delta} \left[\delta^{-1} \ln\left(1 - \exp(-\eta_o)\, P_o^{-1} P_x\right)\right] d\delta \tag{7}$$

which may be easily evaluated numerically (9).

Experimental Details

Titanium specimens of commercial purity (Ti-A55) were vacuum annealed for 100 hours at 1600°F to remove TiH inclusions which had been observed in optical microscopy of the as-received material. Results from wet analysis of a sample after vacuum annealing is given in Table I.

Table I. Wet Analysis of the Vacuum-Annealed Titanium-A55

Fe	.08
C	.02
O	.1384
H	.0076
N	.010
Yt	<.0005
OE	<.10 (Other Elements each)
OET	<.40 (Other Elements Total)
Ti	REMAINDER

Before exposure to oxidizing conditions the titanium surfaces were cleaned in a bath of acetone followed by methanol rinse and were wiped dry. It was noted that specimens that had not been cleaned or had been fingerprinted were a light blue after moderate oxidizing exposures whereas the clean specimens after equivalent exposures were a uniform neutral grey.

The specimens were exposed in tube furnaces open to the lab air. Temperature during exposure was monitored by thermocouples in contact with the specimens. A horizontal furnace was used for short exposures (times up to 9 hours). The samples were placed in the horizontal furnace with the furnace at temperature. After 1 minute the samples were within 80°F of the ultimate temperature and within 5°F after 2 minutes. Consequently, the exposure times reported for the short-exposure specimens are 2 minutes less than the actual time each specimen was in the furnace. Considering the probable 51.4 kcal/mole activation energy for the diffusion of oxygen in titanium, which is a conclusion from this paper, it is unlikely that any significant diffusion occurred during the 2-minute transient.

Long exposures (times greater than 24 hours) were done in a vertical tube furnace with thermocouples near the specimen positioned from the top, bottom, and side. The specimens were placed in the vertical furnace while the furnace was cold. The long heating transients were approximately 1 hour and the exposure time for these specimens is the total time.

Results and Discussion

Table II summarizes the oxidation results. The diffusion coefficients and solubility limits for the various times and temperatures were taken from composition-depth profiles obtained by the method outlined in the Theory section of this paper. The diffraction peaks were collected at the (002) reflection using $CuK\alpha_1$ and a quartz diffracted beam monochromator. In some cases other diffraction geometries, such as $CuK\alpha$ with graphite monochromator and Mo radiation with a Zr filler, were used to complement this data.

Three solubility limits were observed for various times and temperatures. They were 20, 25, and 34 atomic percent. These limits were distinct and the transition from one limit to the next was apparently very quick. Figure 1 shows the time-temperature realms of the three limits. The circles, triangles, and squares respectively mark the times and temperatures at which 20, 25, and 34 atomic percent limits were observed.

Figure 2, which is the composition-depth profile of a specimen exposed for 96 hours at 1100°F, is typical of the depth profiles of the specimens that have just undergone a change in the solubility limit. The steep composition gradient near the interface is, in particular, a common feature of all such specimens. Figure 3 is the composition-depth profile of a specimen exposed for 42 hours at 1200°F. In this specimen the 25 atomic percent solubility limit is well established. Figures 4 and 5 are the diffraction peaks for these two profiles. The asymmetry to the left is due to the 25 atomic percent solubility limit. The lower intensity indicates that the concentration gradient is steep.

When the transition from the 25 to 34 atomic percent solubility limit occurs, steep gradients in the profile and asymmetries in the diffraction peaks are seen. Figure 6 is the composition-depth profile of a specimen exposed for 106 hours at 1400°F. Figure 7 is the diffraction peak for the same specimen; the asymmetry to the left is due to the 34 atomic percent limit.

Table II. Experimental Results From Oxygen Contaminated Ti-A55 Specimens

Sample ID	Diffraction Method	Temp., °F	Time, hours	$D \times 10^{12}$ cm^2 S^{-1}	C_s, atom %	C_o, atom %
11H	Cu/Quartz	1100	1	0.33 ± 0.05	18.8 ± 0.6	0.7 ± 0.4
14H			4	0.25 ± 0.01	19.8 ± 0.2	0.8 ± 0.1
19H			9	0.27 ± 0.02	19.8 ± 0.3	0.9 ± 0.3
196H			96		25	
21H		1200	1	1.75 ± 0.07	19.5 ± 0.2	0.7 ± 0.1
24H			4	1.5 ± 0.1	18.0 ± 0.2	0.7 ± 0.3
29H			9	1.6 ± 0.3	19.2 ± 0.6	0.0 ± 0.8
29H	Cu/Graphite		9	1.6 ± 0.5	18.5 ± 0.7	0 ± 2
242H	Cu/Quartz		42		25	
2103H			103		25	
2592H		1250	92		25	
330M1		1300	0.5	6.8 ± 0.4	21.0 ± 0.3	1.2 ± 0.2
330M2			0.5	7.4 ± 0.5	21.8 ± 0.3	1.4 ± 0.3
348M1			0.8	7.9 ± 0.9	21.6 ± 0.5	1.0 ± 0.5
348M2			0.8	7.4 ± 0.6	21.7 ± 0.3	1.0 ± 0.4
34H			4		25	
SPC 17			34		25	
370H			70		25	
3108H			108		33	
415M1		1400	0.25	36 ± 5	21.2 ± 0.5	0.8 ± 0.5
415M2			0.25	43 ± 6	19.8 ± 0.6	0.6 ± 0.6
430M2			0.5		25	
430M3			0.5		25	
426H			26		33	
4106H			106		33	
4106H	Mo/Zr		106	21 ± 11	32 ± 7	0 ± 3

The increases in the composition gradient associated with the 25 and 34 atomic percent solubility limit imply a compositionally dependent diffusion coefficient. Below 20 atomic percent, however, the diffusion coefficient appears constant. Nonlinear regression was used on specimens with the 20 atomic percent solubility limits to fit their composition-depth profiles to the equation:

$$C = C_o + (C_s - C_o)\ \mathrm{erfc}\left(\frac{x}{2\sqrt{Dt}}\right) \qquad (8)$$

where C is the composition in atomic percent, C_o is the initial oxygen content in atomic percent, C_s is the solubility limit in atomic percent, x is the depth in cm, D is the diffusion coefficient in cm^2/sec, and t is the time in seconds. Figure 8 shows the composition-depth profile for several times and temperatures.

Figure 9 shows the Arrhenius plot of the diffusion coefficient for all specimens having a 20 percent solubility limit. Using linear regression an activation energy of 51.4 ± 0.8 kcal $mole^{-1}$ and an intercept of

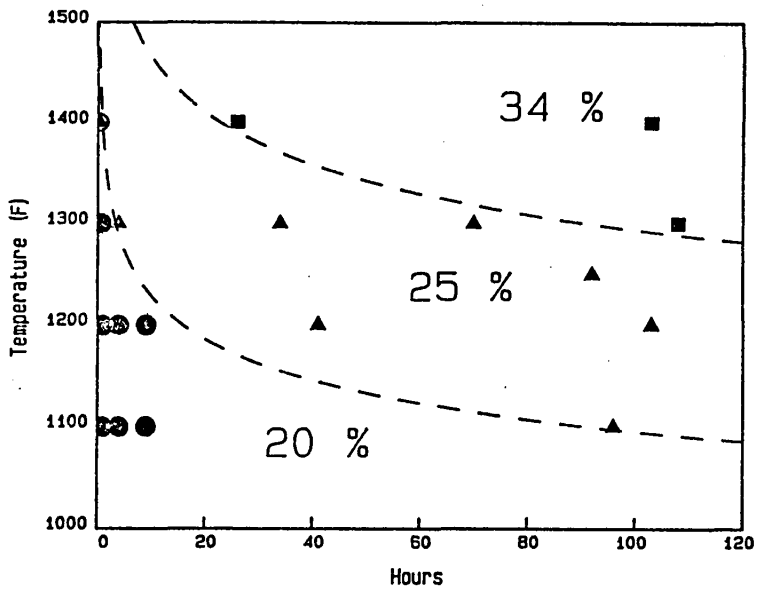

Figure 1. The solubility limit of oxygen in titanium during exposure to air. The limit increases in a stepwise fashion. Observed limits are plotted against time and temperature where circles, triangles, and squares represent the 20, 25, and 34 percent limits, respectively.

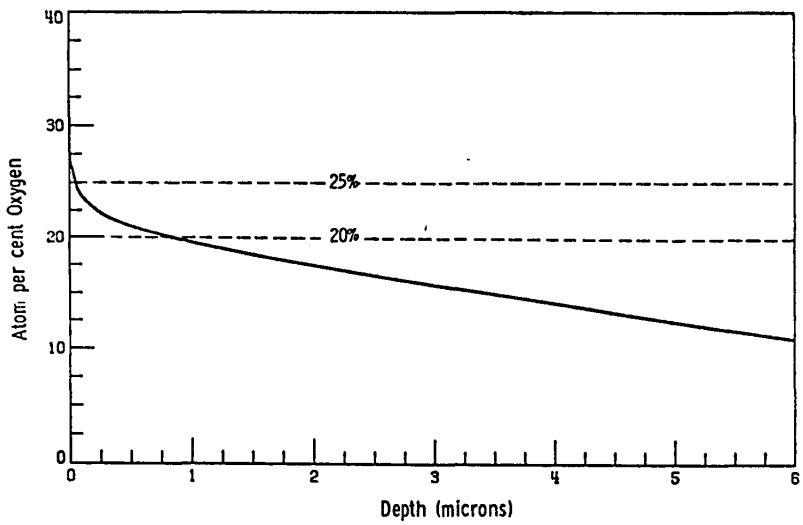

Figure 2. Profile for a 96 hour, 1100°F exposure. The 25 percent solubility limit and the corresponding diffusion limb have probably formed in the final 10 hours of the exposure.

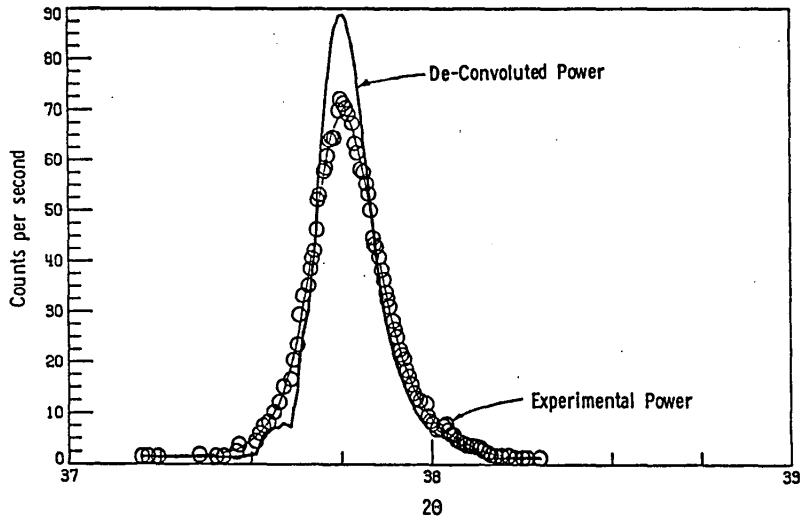

Figure 3. The (002) intensity band for a 96 hour, 1100°F exposure corresponding to the profile in Figure 2. The intensity shoulder to the left of the main peak is due to the 25 percent diffusion limb.

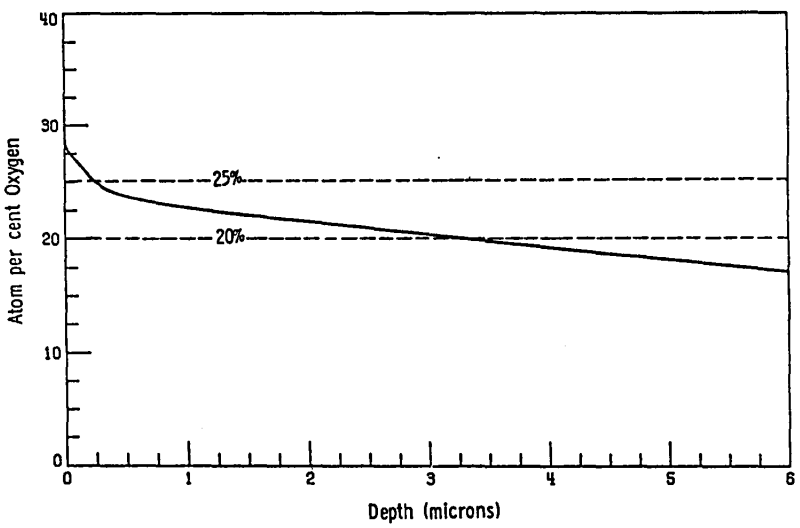

Figure 4. Profile for a 42 hour, 1200°F exposure. The 25 percent solubility limit and the corresponding diffusion limb have probably formed after 12 hours.

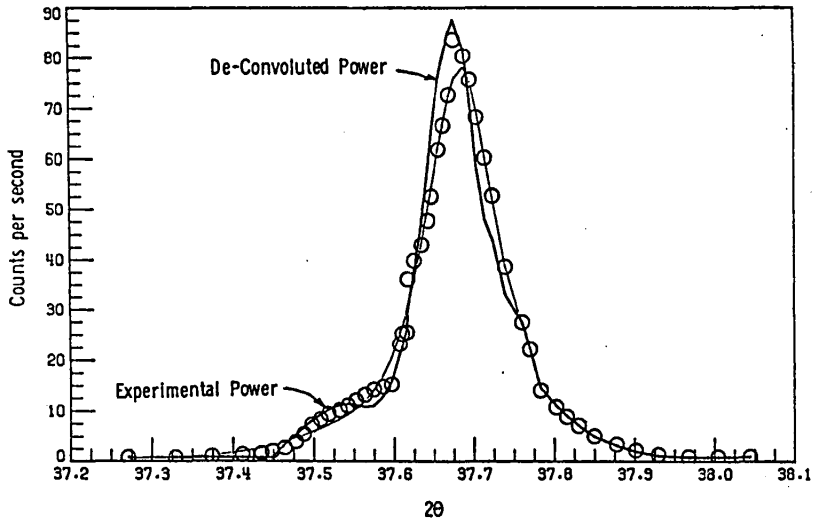

Figure 5. The (002) intensity band for the 42 hour, 1200°F exposure in Figure 4. The intensity shoulder to the left of the main peak is due to the 25 percent diffusion limb.

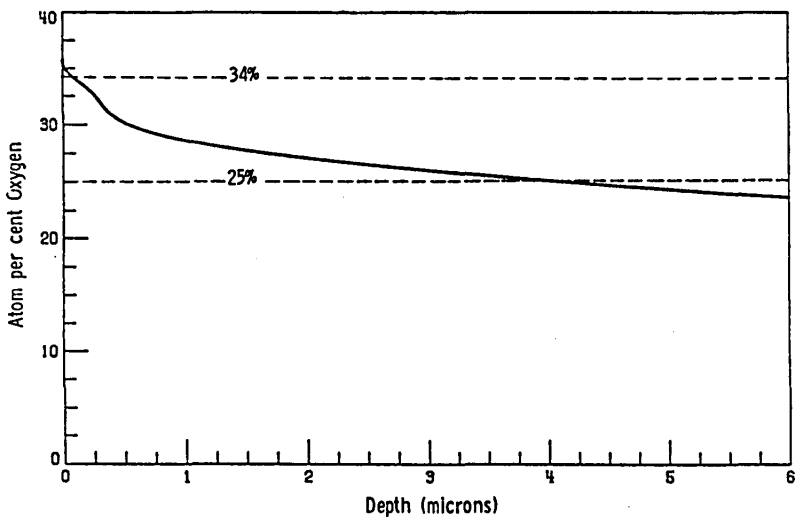

Figure 6. Profile for a 106 hour, 1400°F exposure. The 25 percent limit has probably formed during the first hour and the 34 percent limit has probably formed after 20 hours.

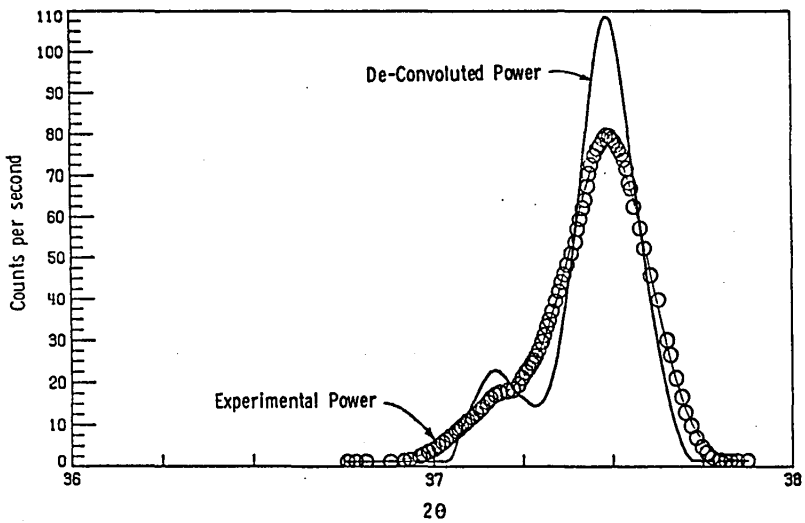

Figure 7. The (002) intensity band corresponding to Figure 6 - a 106 hour, 1400°F exposure. The main peak is due to the 25 percent limit and the shoulder to the left is due to the 34 percent limit.

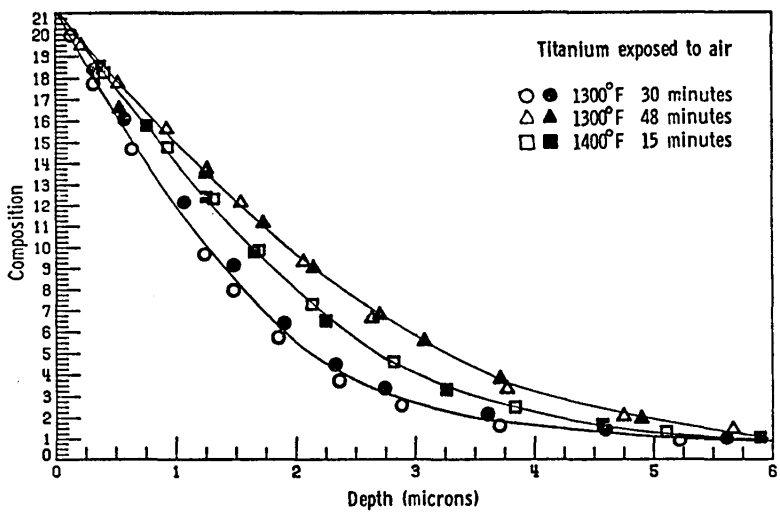

Figure 8. Profiles for three times and temperatures. Replicates were prepared and analyzed independently.

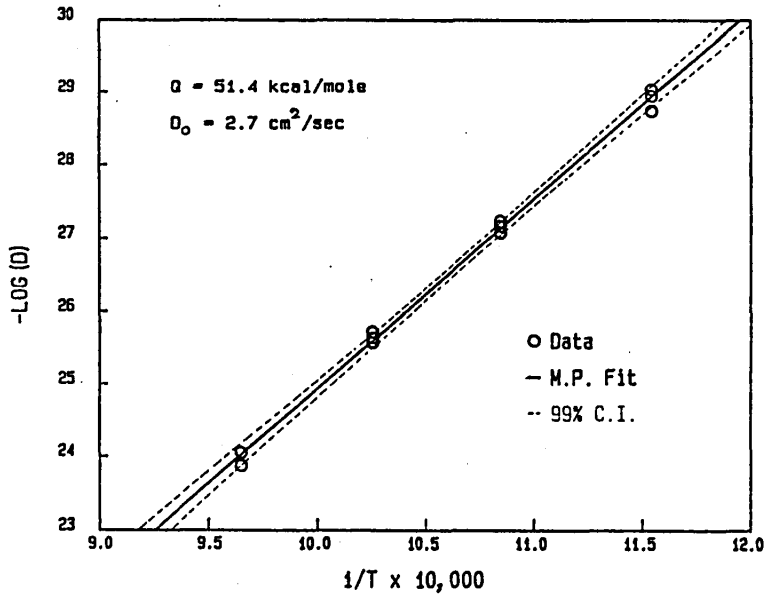

Figure 9. Arrhenius plot of the diffusion coefficient for the 20 percent diffusion limb.

2.7 ± 0.5 cm^2/sec were found. The solid line is the most probable fit and the dashed lines represent the 90 percent confidence limits of the linear regression. The activation energy of 51.4 kcal mole^{-1} is close to the values reported by David et al. (48 kcal mole^{-1}) and Kofstad et al. (51 kcal mole^{-1}). It was determined by trial and error that the equation:

$$C = C_o + (C_s - C_o)\ \mathrm{erfc}\left(\frac{x}{2\sqrt{D_1 t}}\right) + 5\ \mathrm{erfc}\left(\frac{x}{2\sqrt{D_2 t}}\right) + 9\ \mathrm{erfc}\left(\frac{x}{2\sqrt{D_3 t}}\right) \quad (9)$$

where

$$D_1 = 2.7\ \exp(-51400/RT) \quad (10)$$

$$D_2 = 0.02\ \exp(-51400/RT) \quad (11)$$

$$D_3 = 0.0001\ \exp(-51400/RT) \quad (12)$$

fits the data quite well. Equation (9) has no fundamental significance. For most practical purposes the second and third erfc terms can be dropped

as they will not contribute significantly to the diffusion near 1.5 atomic percent, which is the embrittlement composition.

Below 1.5 atomic percent α-titanium is expected to be ductile and above 1.5 atomic percent α-titanium is expected to be brittle (10). The depth of embrittlement is given by the solution of the equation:

$$\left(\frac{1.5 - C_o}{20 - C_o}\right) = \text{erfc}\left(\frac{x}{2\sqrt{D_1 t}}\right) \tag{13}$$

For $0 < C_o < 1$ atomic percent the following approximation is adequate:

$$X_e \sim 2\sqrt{D_1 t}\sqrt{-0.935 - 0.9339 \ln\left(\frac{1.5 - C_o}{20 - C_o}\right)} \tag{14}$$

where X_e is the embrittlement depth. This is dependent on D_1 which is a function of temperature. Therefore, X_e is a function of time and temperature. Figure 10 depicts the embrittlement depth on a composition depth profile for a 25 hour 1400°F exposure.

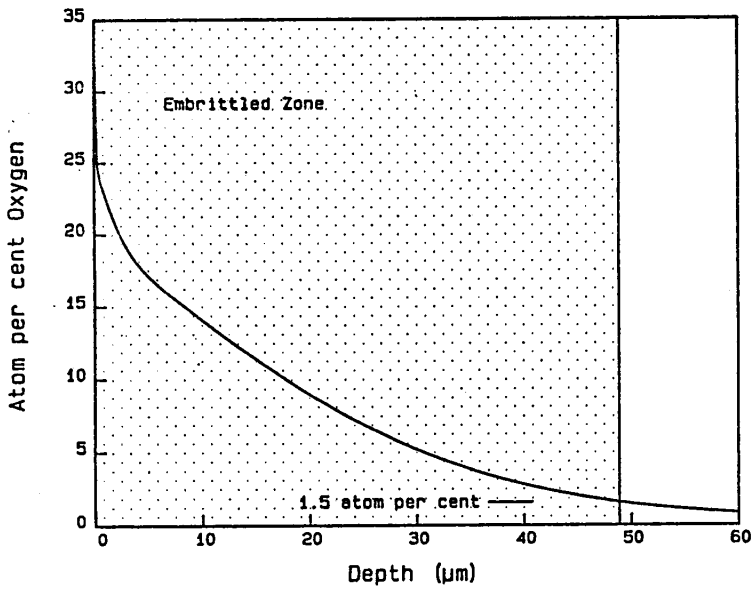

Figure 10. Simulated profile of a 25 hour, 1400°F exposure. The embrittlement depth is defined as the 1.5 atom percent threshold.

The reduction of ductile cross-sectional area in small members is the critical factor in loss of strength. For large members stress intensification due to cracks in the embrittled zone may be more significant than the reduction of cross-sectional area. The times required to produce appreciable crack lengths, however, are very long.

The step behaviour of the solubility limits suggests that there is some time dependent process - such as ordering - which must be completed before the transitions can occur. It is also possible that the 20-25 and 25-34 atomic percent diffusion limbs are too thin to be observed by CuKα. Inasmuch as the linear absorption of CrKα is greater than that of CuKα, investigators of this phenomenon may wish to use Cr radiation instead of Cu. The greater depth resolution near the surface should enable them to observe whether the 25 and 34 atomic percent limits exist at all times or appear abruptly. Similarly, investigators of higher temperatures or longer oxidation times may wish to use Mo or Ag radiation because the linear absorption of MoKα and AgKα are less than CuKα and will therefore penetrate more deeply.

Conclusions

The solubility limit of oxygen in titanium during oxidation is initially 20 atomic percent. Subsequently 25 and 34 atomic percent limits are observed. Three distinct limbs are associated with these three solubility limits. The most rapid diffusion occurs in the limb associated with the 20 percent limit and for most practical purposes the diffusion in the other limbs can be ignored.

Acknowledgements

The authors are grateful to the NASA Langley Research Center for the support of this research.

References

1. E. S. Bumps, H. D. Kessler, and M. Hansen, Transactions Am. Society Metals, 45 (1953), p. 1008.

2. Bo Holmberg, Acta Chem. Scand., 16 (1962), pp. 1255-1261.

3. Sten Anderson, Bengt Collen, Ulf Kuylenstiera, and Arne Magneli, Acta Chem. Scand., 11 (1957), pp. 1641-1652.

4. P. Kofstad, P. B. Anderson, and O. J. Krudtaa, J. Less-Common Metals, 3 (1961), pp. 89-97.

5. Daniel David, Eduardo A. Garcia, Xavier Lucas, and Gerard Beranger, C. R. Acad. Sc. Paris, t.287 (1978) Serie B - 125.

6. J. Unnam, R. N. Shenoy, and R. K. Clark, AIME, Paper no. A84-56 (1984).

7. K. E. Wiedemann, Thesis, Virginia Polytechnic Institute and State University (1983).

8. J. Unnam, J. A. Carpenter, and C. R. Houska, J. Ap. Phys., 44 (1976), p. 1957.

9. K. E. Wiedemann and J. Unnam, LAR-13356, COSMIC, Univ. of Georgia (1984).

10. D. Gupta and S. Weinig, "Transactions of the Metallurgical Society of AIME," 215 (1959), pp. 209-216.

End of Document